Exp Fluids
DOI 10.1007/s00348-008-0567-4

RESEARCH ARTICLE

Dynamic consistent correlation-variational approach for robust optical flow estimation

D. Heitz · P. Héas · E. Mémin · J. Carlier

Received: 24 November 2007 / Revised: 28 August 2008 / Accepted: 1 September 2008

Abstract We present in this paper a novel combined scheme dedicated to the measurement of velocity in fluid experimental flows through image sequences. The proposed technique satisfies the Navier–Stokes equations and combines the robustness of correlation techniques with the high density of global variational methods. It can be considered either as a reenforcement of fluid dedicated optical-flow methods towards robustness, or as an enhancement of correlation approaches towards dense information. This results in a physics-based technique that is robust under noise and outliers, while providing a dense motion field. The method was applied on synthetic images and on real experiments in turbulent flows carried out to allow a thorough comparison with a state of the art variational and correlation methods.

1 Introduction

There has been significant progress during recent years in the analysis of particle image sequence to estimate fluid velocities. On one hand regions-based techniques produce velocities from maximum correlations between displaced interrogation windows. These robust techniques provide reliable but low-pass filtered vector fields, compared to the density of particles. On the other hand *model based measurement* techniques, known as optical flow approaches, rely on a model, the so-called data term or observation term, which relates the observed image intensity to the displacements fields to estimate. Since the single use of the data term leads to an improperly posed problem—only the displacements along the direction of the intensity gradient can be measured—additional assumptions have been proposed. The *local* approach of Lucas and Kanade (1981) tackles this problem while considering a local spatial constancy assumptions on the optic flow field. Bigün and Granlund (1988) extended this technique to local spatiotemporal constancy assumptions. Like correlation approaches, these *local* schemes are region-based methods, providing robust but sparse estimations.

Alternatively, a relatively simple important idea in the conceptual development of model-based measurement technique is to introduce a regularization of the velocity field to devise a *global* approach (Tikhonov and Arsenin 1977). Based on the minimization of an energy function, composed of a data term and a regularization term, this *global* scheme provides dense vector fields with spatial coherence. It should be noticed, that contrary to approaches using post-treatments to filter spurious vectors, *global* approaches seek regular and coherent displacements fields. This promotion of regular and coherent solutions is conducted from the beginning of the minimization. Hence, the key of *global* methods's accuracy is directly link with the regularization term. However, these approaches provides a framework to introduce physics-based constraints, thus giving opportunities to introduced prior knowledges of the dynamics of fluids to extract the

D. Heitz · P. Héas · J. Carlier
Cemagref, UR TERE, 17 Avenue de Cucillé, CS64427,
35044 Rennes, France

D. Heitz (✉) · P. Héas · J. Carlier
Université Européenne de Bretagne, Rennes, France
e-mail: dominique.heitz@cemagref.fr

Present Address:
P. Héas · E. Mémin
INRIA, Campus Universitaire de Beaulieu, 35042 Rennes,
France

motion through image sequences. In this paper we examines new physics-based constraints leading to dynamic consistency.

The *global* scheme proposed by Horn and Schunck (1981), using the optical flow constraint equation (OFC), and a first-order regularization, was applied on particle image by Ruhnau et al. (2005). However, this standard approach was at the origin adapted to two-dimensional (2D) rigid motions. With particle image of turbulent fluid flows, the OFC equation—based on the variational formulation of the brightness constancy assumption—is violated due to out of plane motions, and the regularization promotes smooth vector fields. The fluid dedicated approach of Corpetti et al. (2002) uses a data term based on the continuity equation and a second-order regularizer constraining the gradients of the flow components divergence and vorticity. This new method is able to extract the apparent 2D motion of 3D flow while preserving the spatial variations of the apparent divergence and vorticity. Applied to particle images it provides reliable results (Corpetti et al. 2006). The optical flow method used by Corpetti et al. based on the continuity equation is physically consistent only for transmittance images. Recently, Liu and Shen (2008) gave the mathematical definition and a physical meaning of this optical flow formulation for particle images. They showed that the continuity equation fortunately leads to the physics-based data term they derived, with the assumption that the boundary flux terms can be neglected for particle images.

The accuracy of second-order regularization was improved with carefully designed Helmholtz decomposition (Kohlberger et al. 2003) and discrete orthogonal decomposition (Yuan et al. 2007). For 2D flows this last method provides better results than advanced competitive correlation approaches (Heitz et al. 2008). To obtain an accurate estimation of the derivatives of the velocity, Alvarez et al. (2008) proposed an optical flow approach based on a second-order Taylor development of the flow. In this technique the physical meaning was enhanced with decomposition of the velocity gradient tensor into symmetric and antisymmetric parts, thus exhibiting the vorticity and strain rate tensor. Recently, Rhunau and Schnörr (2007) devised a physically grounded regularization based on the Stokes equation, therefore restricted to viscous flow (i.e. for very small Reynolds numbers).

Another way to introduce physics in the estimation of motion is to satisfy the Navier–Stokes equations. This approach was first introduced by Okuno et al. (2000) to post-treat standard correlation measurements. Like the method of Rhunau and Schnörr (2007), this physic-based measurement technique provides estimations of the velocity and of the pressure. Using the incompressible velocity–vorticity formulation of the Navier–Stokes equations, Rhunau et al. (2007) developed a spatio-temporal regularizer for a *global* approach equipped with an additional constraint that mimics the small viscous term. In the context of data assimilation into Navier–Stokes equations, Cuzol et al. (2007) presented a Bayesian filtering technique to track vorticity fields, and Papadakis et al. (2007) proposed a promising variational data assimilation technique to estimate an optimal dynamically consistent vector fields. All the above-mentioned spatio-temporal techniques are only valid for 2D flows, which represents a strong limitation for the analysis of most of real flows.

Furthermore, variational approaches can exhibit other limitations with particle image sequences. The variational formulation is only suited for displacements smaller than the shortest wavelength present in the image, i.e. smaller then the size of the observed particles. To handle large displacements the data term is generally embedded within a multiresolution coarse-to-fine scheme (Bergen et al. 1992). Standard multiresolution approach consists in deriving the original frame into a pyramid of images, by successive low-pass filtering (Gaussian smoothing) and regular subsampling by a factor of two in each direction. The created pyramid structure then allows multiscale motion estimation by incremental procedure. Low resolution components are estimated at coarsest level and then refined step by step: at a resolution level, an increment velocity field is estimated around the projection (by duplication or interpolation) of the final estimate at previous resolution level. In general the procedure of filtering and subsampling leads to a loss of information. In the case of particle images of turbulent fluid flows, small particles with large velocities, can be smoothed out by the multiresolution procedure. Therefore, due to this loss of information, the variational approach will not extract reliable velocities. In presence of noise in the image the multiresolution procedure enhances this phenomenon. At the coarsest level, the subsampling process keeps statistically more noise than particle information when there is poor particle density and noise in the original image. Bruhn et al. (2005) proposed a combined local–global method which has the robustness of local methods with the density of global approaches. Unfortunately, this technique, not specifically suited for fluid flow, was not tested on particle images.

In the present paper we describe a novel dynamic consistent *global* approach combining the robustness of correlation techniques with the high density of global variational methods, constrained with Navier–Stokes equations extending the estimations towards 3D flows driven by shallow water equations. The proposed approach is an adaptation of Héas et al. (2007) scheme—developed for the measurement of atmospheric dynamics from satellite image sequences—for laser sheet illuminated particle image. This results in a physics-based technique that is

robust under noise and outliers, while providing a dense spatio-temporal coherent motion field.

This article is organized as follows. In Sect. 1, we present multiscale motion estimation focusing on the fluid dedicated variational methods. Then, in Sect. 2, we present the collaborative correlation-variational approach, followed by the description of spatio-temporal constraint. In Sect. 6, results from synthetic images based on a DNS of 2D turbulence, and real images in the wake of a circular cylinder, are presented and analyzed. We provide some elements of comparison of our method with standard optical flow techniques.

2 Multiscale motion estimation

2.1 Regions-based or local approach

A classical approach used with PIV is correlation-based matching technique. The velocity $\mathbf{u}$ at point $\mathbf{s}$ is obtained for continuous image fields by minimizing

$$\mathbf{u}(\mathbf{s}) = \Delta t^{-1} \arg\min_{\mathbf{w}} \int_{\mathbf{r}\in W(\mathbf{s})} -I(\mathbf{r}+\mathbf{w}, t+\Delta t) I(\mathbf{r}, t) \mathrm{d}\mathbf{r}. \quad (1)$$

where $W(\mathbf{s})$ denotes windows centered on different points of the images and $\mathbf{w}$ is the displacement vector to estimate. For *local* optical flow approaches, which belong to regions-based methods, the negative product of the images is replaced by the absolute value or the square of the DFD equation (see Sect. 2.2).

These approaches suffer from several deficiencies: traceable features must be sufficiently contrasted and must persist over time on consecutive images. Furthermore, the estimation prone to erroneous spatial variability, which can be reduced with the use of filters. On the other hand, these techniques constitute very fast methods and are generally locally very robust to noise. These techniques are based on disjoint local estimation, and thus produce sparse vector fields estimated locally and independently.

2.2 Global or dense approach

2.2.1 Classical optical flow method

The apparent motion, perceived through variations of image intensity I is called *optical flow* in the computer vision community. All optical flow estimation methods rely on the temporal conservation of some invariants. The most common are photometric invariant which can easily be extracted and may lead to dense measurements. In the case of PIV of bi-dimensional flows, the gray level conservation can be assumed, leading to an integrated non-linear formulation called the displaced frame difference (DFD) equation $I(\mathbf{s}+\mathbf{u}(\mathbf{s}),\ t+\Delta t) = I(\mathbf{s},\ t)$, or at time t, to a linear differential formulation called the OFC equation $\mathbf{u}(\mathbf{s}) \cdot \nabla I(\mathbf{s}) + I_t(\mathbf{s}) = 0$, where $\mathbf{s}$ denotes the spatial coordinates (x, y) and $\mathbf{u}(\mathbf{s}) = (u, v)^T$ the apparent motion field at this point and at a given time t.

These two formulations cannot be used alone, as they provide only one equation for two unknowns at each spatio-temporal location $(\mathbf{s}, t)$. This is the well-known *aperture problem* where the normal flow to the brightness gradient is estimated while the tangential velocity component remains undetermined. In order to remove this ambiguity one must rely on other assumptions. The mainly used assumption is *local* spatial or spatio-temporal constancy of the velocity fields (Lucas and Kanade 1981; Bigün and Granlund 1988).

Alternate approaches, derived in the framework proposed by Horn and Schunck (1981), have the great advantage of producing dense vector fields with spatial *global coherence*. They are based on the minimization of an energy function $J = J_\mathrm{d} + J_\mathrm{r}$ composed of two terms. The first term J_d is called the data term and implements the OFC equation

$$J_\mathrm{d}(\mathbf{u}, I) = \int_\Omega \phi\left[\nabla I(\mathbf{s}) \cdot \mathbf{u}(\mathbf{s}) + \frac{\partial I(\mathbf{s})}{\partial t}\right] \mathrm{d}\mathbf{s}. \quad (2)$$

The penalty function ϕ is usually the L_2 norm but it may be changed to a robust function attenuating the effect of data that deviate significantly from the OFC (Black and Anandan 1996). The second term J_r is called the regularization term. It is usually a standard first-order spatial smoothness term

$$J_\mathrm{r}(\mathbf{u}) = \alpha \int_\Omega \phi(\| \nabla u \| + \| \nabla v \|) \mathrm{d}\mathbf{s}, \quad (3)$$

where $\alpha > 0$ is a parameter controlling the balance between the smoothness and the global adequacy to the brightness constancy assumption. $\|\cdot\|$ stands for the Euclidean norm. Function ϕ may be the quadratic penalty if the searched solution is smooth everywhere or a robust norm function if one wants to handle implicitly the spatial discontinuities of the field (Black and Anandan 1996).

2.2.2 Fluid dedicated optical flow method

With most of real turbulent flows, the OFC equation dose not hold. To estimate the apparent motion (i.e. the velocity in the image plane) of 3D flows, Corpetti et al. (2002, 2006) proposed a data term based on the continuity equation. This new constraint although derived for transmittance images is fortunately suited for laser-sheet illuminated particle images (Liu and Shen 2008). Liu and Shen demonstrated that the optical flow is proportional to the path averaged velocity

of particles across the laser sheet and proposed the following physics-based optical flow equation,

$$\nabla(I(\mathbf{s})\cdot\mathbf{u}(\mathbf{s}))+\frac{\partial I(\mathbf{s})}{\partial t}=f(\mathbf{s},I), \tag{4}$$

$$f(\mathbf{s},I)=D\nabla^2 I+DcB+c\mathbf{n}\cdot(N\mathbf{u})|_{\Gamma_1}^{\Gamma_2}, \tag{5}$$

where D is a diffusion coefficient, c is a coefficient of particle scattering/absorption, $B=-\mathbf{n}\cdot\nabla N|_{\Gamma_1}^{\Gamma_2}-\nabla\cdot(N|_{\Gamma_2}\nabla\Gamma_2+N|_{\Gamma_1}\nabla\Gamma_1)$ is a boundary term that is related to N, the particle number per unit total volume, and its derivatives coupled with the derivatives of the control surfaces Γ_1, Γ_2 of the laser sheet illuminated volume. Since the control surfaces are planar, there is no particle diffusion by molecular process, and the rate of accumulation of the particle in laser sheet illuminated volume is neglected, the term $f(\mathbf{s}, I)\simeq 0$ and the physics-based OFC can be written

$$J_{\mathrm{d}}(\mathbf{u},I)=\int_{\Omega}\phi\left[\nabla(I(\mathbf{s})\cdot\mathbf{u}(\mathbf{s}))+\frac{\partial I(\mathbf{s})}{\partial t}\right]\mathrm{d}\mathbf{s}. \tag{6}$$

Furthermore in the case of fluid flows, it can be demonstrated that a first-order regularization is not adapted as it favors the estimation of velocity fields with low vorticity (Corpetti et al. 2006). A second-order regularization can advantageously be considered as proposed by Suter (1994):

$$J_{\mathrm{r}}(\mathbf{u})=\alpha\int_{\Omega}\phi(\|\nabla\xi(\mathbf{s})\|^2+\|\nabla\zeta(\mathbf{s})\|^2)\mathrm{d}\mathbf{s}, \tag{7}$$

where $\xi=\mathrm{curl}\,\mathbf{u}=\frac{\partial u}{\partial y}-\frac{\partial v}{\partial x}$ and $\zeta=\mathrm{div}\,\mathbf{u}=\frac{\partial u}{\partial x}+\frac{\partial v}{\partial y}$ stand for the vorticity and divergence of the apparent velocity $\mathbf{u}=(u,\ v)^T$. Note that in the case of bi-dimensional incompressible flows, divergence of the apparent motion is equal to zero. High-order regularization leads to non-trivial minimization problems. As a consequence more sophisticated discretization schemes have to be used. Using finite mimetic differences, Yuan et al. (2007) proposed a high-order motion estimator providing accurate measurements (Heitz et al. 2008).

In the present study, to circumvent the difficulty of implementing second-order smoothness constraint, the second-order regularization term was simplified in a computational point of view in two interleaved first-order div–curl regularizations based on auxiliary variable ξ_1 and ζ_1 approximating the vorticity and the divergence of the flow (Corpetti et al. 2002, 2006). Thus we have:

$$J_{\mathrm{r}}(\mathbf{u})=\alpha\int_{\Omega}\phi[(\xi(\mathbf{s})-\xi_1)^2+\lambda\|\nabla\xi_1\|^2]\mathrm{d}\mathbf{s} \tag{8}$$

$$+\alpha\int_{\Omega}\phi[(\zeta(\mathbf{s})-\zeta_1)^2+\lambda\|\nabla\zeta_1\|^2]\mathrm{d}\mathbf{s}, \tag{9}$$

where λ is a positive regularization parameter. Although Yuan et al. (2007) numerical scheme provides better results, here the Corpetti et al. regularization is used for simplicity.

2.3 Multiresolution approach

A problem with variational approaches is large displacement estimation. The intensity function must be locally sufficiently close to a linear function. Since the larger the displacement the more narrow the linearity domain is, large displacements cannot be recovered directly. A common way to overcome this limitation is to create a image pyramid, constructed by successive low-pass filtering and down sampling of the original images. In this framework, principal components of displacements are first estimated at coarse resolution where motion amplitude should be sufficiently reduced in order to satisfy the linearity requirement. Incremental displacement are then estimated while going down the pyramid, and the solution is refined (Bergen et al. 1992) (Fig. 1).

The multiresolution schemes estimates principal component displacements only at coarse resolutions where small particles are rubbed out. Hence, this approach enables the characterization of large displacements of small particles only in the case when their motion are close enough to the principal component's one. Since at the coarsest level, the subsampling process keeps statistically more noise than particle information, especially when there is poor particle density or small particles (around 1–2 pixel diameter) and noise in the image, the multiresolution approach leads to erroneous estimations.

3 Collaborative correlation-optical flow scheme

To overcome the multiresolution limitations, we propose an alternative approach relying on a unique representation of the full resolution image. Thus, the proposed method

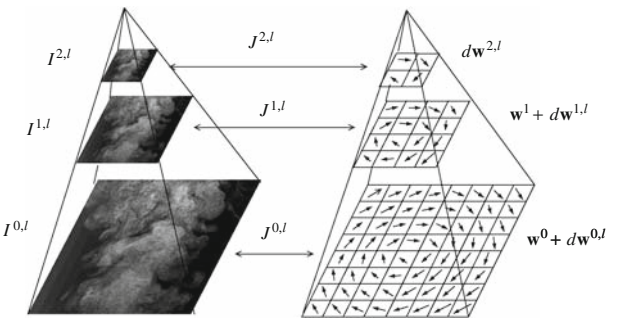

Fig. 1 Coarse to fine resolution with multiresolution representation of the images

tackles the non-linear estimation problem without making successive approximations in the calculation of interpolated images nor restricting itself to the characterization of large displacements of sufficiently large structures. The proposed method takes advantage of the non-linear formulation of the motion estimation problem within a differential framework appropriated for globalized local smoothing. More explicitly, large displacements of both, fine or large structures, can be recovered by correlation-based methods for sufficiently contrasted and persisting image regions. Thus, the idea of the method is to replace the coarse estimates of the multiresolution scheme by a dense large scale displacement estimate derived from a collection of correlation-based vectors $\mathbf{u}_c$ obtained by Eq. 1.

A new functional was defined to estimate the vector fields

$$J(\mathbf{u}) = J_d(I, \mathbf{u}) + J_r(\mathbf{u}) + J_c(\mathbf{u}, \mathbf{u}_c), \tag{10}$$

where $J_c(\cdot)$ is the energy function constraining estimated displacements $\mathbf{u}$ to be close to a sparse correlation-based vector field $\mathbf{u}_c$. Thus, functional $J_c(\cdot)$ is defined as a quadratic distance between the solution and a collection of correlation-based vectors $\mathbf{u}_c^i = (u^i, v^i)$ located at the point $\mathbf{s}^i = (x^i, y^i)$ and influencing their neighborhood according to a bi-dimensional Gaussian $\mathcal{N}^i(\mathbf{s})$ of mean $\mathbf{s}^i$ and of variance σ

$$J_c(\mathbf{u}, \mathbf{u}_c) = \gamma \int_\Omega \sum_{i=1}^{L} g^i \mathcal{N}^i(\mathbf{s}) \parallel \mathbf{u}_c^i - \mathbf{u}(\mathbf{s}) \parallel^2 \mathrm{d}\mathbf{s}, \tag{11}$$

where g^i and γ denote respectively the confidence and the functional weighting factors.

4 Spatio-temporal smoothing

4.1 Energy function

We propose to incorporate a priori physical knowledge on fluid dynamical evolution in the combined correlation-optical flow estimation scheme. In order to preserve spatio-temporal consistency of displacement estimates, a simplified Navier–Stokes dynamical model is adapted to images depicting 3D fluid flows. A dense displacement field is predicted by time integration of a physical dynamical model. The propagated field is then introduced in the estimation process as a spatio-temporal smoother. A priori information introduced with this dynamic model may enhance significantly the quality of estimates especially in the case of noisy observations.

Keeping notations of the previous section, we define for the estimation of variable $\mathbf{u}$ the new functional

$$J(\mathbf{u}, I) = J_d(\mathbf{u}, I) + J_r(\mathbf{u}) + J_p(\mathbf{u}, \mathbf{u}_p) + J_c(\mathbf{u}, \mathbf{u}_c), \tag{12}$$

where $J_p(\cdot)$ is an energy function constraining displacements $\mathbf{u}$ to be consistent with a physically sound prediction $\mathbf{u}_p$ relying on Navier–Stokes equations. As proposed in Héas et al. (2007), we define this functional as a quadratic distance between the estimated field $\mathbf{u}$ and the dense propagated field $\mathbf{u}_p = (u_p, v_p)$:

$$J_p(\mathbf{u}, \mathbf{u}_p) = \beta \int_\Omega \parallel \mathbf{u}_p(\mathbf{s}) - \mathbf{u}(\mathbf{s}) \parallel^2 \mathrm{d}\mathbf{s}, \tag{13}$$

where β denotes a weighting factor. This approach constitutes an alternative to the spatio-temporal smoother defined in Weickert and Schnörr (2001) and is to some extent similar to the temporal constraint introduced in Rhunau et al. (2007). It is important to distinguish this a priori dynamical model from the model used for the data-term. Indeed, from the probabilistic point of view, minimizing the functional is analogous to searching the maximum a posteriori estimate obtained by maximizing the product of the likelihood probability distribution represented by the data-term and a priori probability distribution represented by spatio-temporal smoothing.

4.2 Dynamical model

Dynamical models describing motion field evolution are needed here for the prediction at time $t + \Delta t$ of a motion field $\mathbf{u}_p$ using the previous estimation performed between time $t - \Delta t$ and t. In Weickert and Schnörr (2001), the temporal derivative of the velocity vectors are constrained to be weak, which is not consistent with fluid flow dynamics. The smoothing proposed in Rhunau et al. (2007) constrains the estimated vorticity to be close to a prediction. Relying on Navier–Stokes equations adapted to shallow flows, the propagation model in Héas et al. (2007) extends this 2D case to flows driven by a shallow water evolution law.

In the present paper we chose to use the latter simplified dynamical model for short time propagation of shallow fluid motion and adapt it to laser-sheet illuminated particle image. Let us present this evolution model. We assume incompressibility of the flow of constant density ρ_0. Denoting respectively by $\mathcal{F} = (\mathcal{F}_u, \mathcal{F}_v)^\top$, $\mathcal{T} = (\mathcal{T}_u, \mathcal{T}_v)^\top$, the viscous forces and turbulent dissipation at subgrid scales the horizontal momentum equations read:

$$\begin{cases} \frac{\mathrm{d}u}{\mathrm{d}t} + \frac{\bar{p}_x}{\rho_0} = \mathcal{F}_u + \mathcal{T}_u \\ \frac{\mathrm{d}v}{\mathrm{d}t} + \frac{\bar{p}_y}{\rho_0} = \mathcal{F}_v + \mathcal{T}_v \end{cases} \tag{14}$$

where the unknown quantities are the pressure function p and horizontal motion field $\mathbf{u} = (u, v)$. An integrated form of the momentum equations is produced by vertical integration. It yields to the shallow water momentum

equations of Saint-Venant (1871). However, a simplified model of these equations can be obtained when relying on the approximation that the vertical profile of horizontal motion is constant within the flow. In other words, we neglect horizontal motion vertical derivatives. By adding the mass conservation model, we form a simplified shallow water system which reads:

$$\begin{cases} \mathbf{u}_t + \nabla(\mathbf{u})\mathbf{u} - g\nabla h = \mathcal{F} + \mathcal{T} \\ h_t + \mathbf{u}\cdot\nabla h + h\nabla\cdot\mathbf{u} = 0, \end{cases} \tag{15}$$

where h denotes the depth function, here the thickness of the laser sheet. Consequently, denoting by ν and ν_s the kinematic viscosity and a subgrid turbulent viscosity, $\mathcal{F}$ and $\mathcal{T}$ are replaced by diffusion terms in the above momentum equations. Let us denote the vorticity by $\xi = \mathrm{curl}(\mathbf{u})$ and the divergence by $\zeta = \mathrm{div}(\mathbf{u})$. The previous system may be expressed in its vorticity-divergence form:

$$\begin{cases} \xi_t + \mathbf{u}\cdot\nabla\xi + \xi\zeta = (\nu_s + \nu)\Delta\xi \\ \zeta_t + \mathbf{u}\cdot\nabla\zeta + \zeta^2 - 2|J| - g\Delta h = (\nu_s + \nu)\Delta\zeta \\ h_t + \mathbf{u}\cdot\nabla h + h\zeta = 0 \end{cases} \tag{16}$$

where $|J|$ is the determinant of the Jacobian matrix of variables $(u,\ v)$, $\nu_s = (C\Delta_x)^2|\xi|$ is the enstrophy-based subgrid scale model proposed by Mansour et al. (1978), and C the Lilly's universal constant equal to 0.17.

For laser-sheet illuminated images of turbulent flows, the thickness of the laser sheet is constant in space and time. Hence, the vorticity-divergence equations provide a dynamical model independent of variable h. Based on the realistic assumption that in 3D flows the divergence of the apparent motion is not weak due to out of plane motions, the simplified vorticity-divergence model based on shallow flows reads:

$$\begin{cases} \xi_t + \mathbf{u}\cdot\nabla\xi + \xi\zeta = (\nu_s + \nu)\Delta\xi \\ \zeta_t + \mathbf{u}\cdot\nabla\zeta + \zeta^2 - 2|J| = (\nu_s + \nu)\Delta\zeta \end{cases} \tag{17}$$

This model for shallow flows reduces in the 2D incompressible case to the vorticity equation:

$$\xi_t + \mathbf{u}\cdot\nabla\xi = (\nu + \nu_s)\Delta\xi. \tag{18}$$

4.3 Algorithm of resolution

The curl and divergence completely determine the underlying horizontal velocity field and the current velocity estimate can be recovered from these quantities up to a laminar flow. Indeed, denoting the orthogonal gradient by $\nabla^\perp = (-\partial/\partial y, \partial/\partial x)^\top$, the Helmholtz decomposition of the field into a sum of gradients of two potential functions is expressed as

$$\mathbf{u} = \nabla^\perp\Psi + \nabla\Phi + \mathbf{u}_{\mathrm{har}}, \tag{19}$$

where $\mathbf{u}_{\mathrm{har}}$ is a harmonic transportation part ($\mathrm{div}\ \mathbf{u}_{\mathrm{har}} = \mathrm{curl}\ \mathbf{u}_{\mathrm{har}} = 0$) of the field $\mathbf{u}$ and where the stream function Ψ and the velocity potential Φ correspond to the solenoidal and the irrotational part of the field. The latter are linked to divergence and vorticity through two Poisson equations. Expressing the solution of both equations as a convolution product with the 2D Green kernel G associated with the Laplacian operator: $\Psi = G * \xi$, $\Phi = G * \zeta$, the whole velocity field can be recovered with the equation

$$\mathbf{u} = \nabla^\perp(G * \xi) + \nabla(G * \zeta) + \mathbf{u}_{\mathrm{har}}, \tag{20}$$

which can be efficiently solved in the Fourier domain. The harmonic transportation component $\mathbf{u}_{\mathrm{har}}$ is recovered by subtracting to the field $\mathbf{u}$ its solenoidal and irrotational parts.

Let us sum up this prediction process. The vorticity and the divergence fields are developed in time in between consecutive image frame using a discretized form of Eq. 17 and time increments δt. After each time increment, assuming $\mathbf{u}_{\mathrm{har}}$ constant within each frame interval, Eq. 20 is used to update the velocity $\mathbf{u}$ needed by Eq. 17, with the current vorticity and divergence estimates. To avoid instability, a semi-implicit first-order upwind time discretization scheme is used to integrate forward Eq. 17. Classical second-order centered finite difference schemes are used for the curl and divergence discretization. To solve the linear system associated with the semi-implicit discretization scheme, the matrix has been constrained to be diagonally dominant, which is a sufficient condition for a well-conditioned inversion problem. This condition reads $1/\delta t \geq \max_s(|u| + |v| - |\xi|)$. Finally, the dynamical model time integration procedure results in the predicted horizontal motion field $\mathbf{u}_p$.

The global algorithm to estimate dynamic consistent multiscale motions is presented in Fig. 2

5 Numerical and experimental evaluation

This section compares results on synthetic and real image sequences obtained with the following approaches:

- *Correlation* To estimate correlation-based velocity fields, the commercial software DaVis 7.2 from LaVision was used. A multipass algorithm with a final interrogation window size of 16 × 16 pixels and 50% overlapping was applied. Image deformation and round Gaussian weighting function were used. Spurious velocities were identified with median filter and replaced by the median. The vector fields obtained

From time index t to the last image index:
- $I(t)$ and $I(t+\Delta t) \leftarrow$ read particle images
- $\mathbf{u}_c(t) \leftarrow$ extraction of a correlation-based vector field with Eq. 1
- $\mathbf{u}(t) = 0, \tilde{I}(t) = I(t+\Delta t)$
- $\mathbf{u}(t) \leftarrow$**Dynamic consistent multiscale** motion estimation
  - Introduction of functionals $J_p(.)$ and $J_c(.)$
  - Until convergence (alternate multigrid optimization) :
    - $\mathbf{u}(t) \leftarrow$ GS(Eq. 12)[1] w.r.t. $\mathbf{u}(t)$
    - $\xi \leftarrow$ GS(Eq. 12) w.r.t. ξ
    - $\zeta \leftarrow$ GS(Eq. 12) w.r.t. ζ
    - $\tilde{I}(t) \leftarrow$ compensate image $I(t+\Delta t)$ with $\mathbf{u}(t)$
- $\mathbf{u}_p(t+n\Delta t) \leftarrow$ **Propagation** of $\mathbf{u}(t)$
  - From time index t to $t+n\Delta t$ with time steps δt
    - ξ and $\zeta \leftarrow$ via Eq.17, $\mathbf{u}(t)$ or $\mathbf{u_p}(t)$
    - $\mathbf{u_p}(t+\delta t) \leftarrow$ via Eq.20, ξ and ζ

[1]"GS(Eq. 12)" denotes a Gauss-Seidel iteration used for the minimization of Eq. 12. Note that in this algorithm the robust parameter estimation steps have been omitted for clarity.

Fig. 2 Synthetic algorithm for dynamic consistent multiscale motion estimation

with this correlation technique were used in the collaborative approach.

- *Dynamic consistent correlation (this paper)* This approach is a filtering process of the correlation via a second-order regularization and a dynamic consistency satisfying the Navier–Stokes equations. This physics-based post-treatment, obtained without the data term in Eq. 12, provides a dense vector field (1 vector per pixel).
- *Multiresolution* (Corpetti et al. 2006) This fluid dedicated optical flow approach uses second-order regularization and multiresolution to handle large displacements (see Sect. 2.2 for details).
- *Dynamic consistent multiresolution (this paper)* This approach is an extension of the fluid dedicated approach of Corpetti et al. (2006) with a spatio-temporal constraint satisfying the Navier–Stokes equations.
- *Correlation variational (this paper)* This collaborative approach is an adaptation of Corpetti et al. (2006) approach to handle large displacements with correlation instead of multiresolution.
- *Dynamic consistent correlation-variational (this paper)* As described above, this approach uses second-order regularization, correlation to handle large displacements and dynamic consistency satisfying Navier–Stokes equations.

For all approaches the same set of parameters was used, providing an optimal performance: $\alpha = 1{,}000$, $\beta/\alpha = 1$ with $\sigma = 8$ pixels and $\gamma/\alpha = 0.05$.

5.1 Synthetic image sequence

To evaluate the performance of the collaborative approach compare to state of the art optical-flow and correlation approaches, a synthetic particle image sequence was generated based on the direct numerical simulation (DNS) of 2D turbulent flow (Carlier and Wieneke 2005). The present flow contains typical difficulties for image-based measurements techniques, like high velocity gradients and large dynamic range. The Reynolds number based on the length scale of domain of computation 2π and on the rms of the forcing velocity was equal to 30,000. Figure 3 presents the whole flow domain and the region considered for a thorough comparison.

The image sequence was generated with a home-made particle image generator involving comparable methods than those developed for the EUROPIV Synthetic Image Generator (Lecordier and Westerweel 2003). A velocity–vorticity formulation of the Navier–Stokes equations was adopted for the DNS. The vorticity equation was solved in Fourier space using desaliased Fourier expansions in two directions with periodic boundary conditions. The time integration was third-order/three steps with a Runge–Kutta scheme. The code is called pseudo-spectral. The coordinates of each particles were calculated in the physical space inside

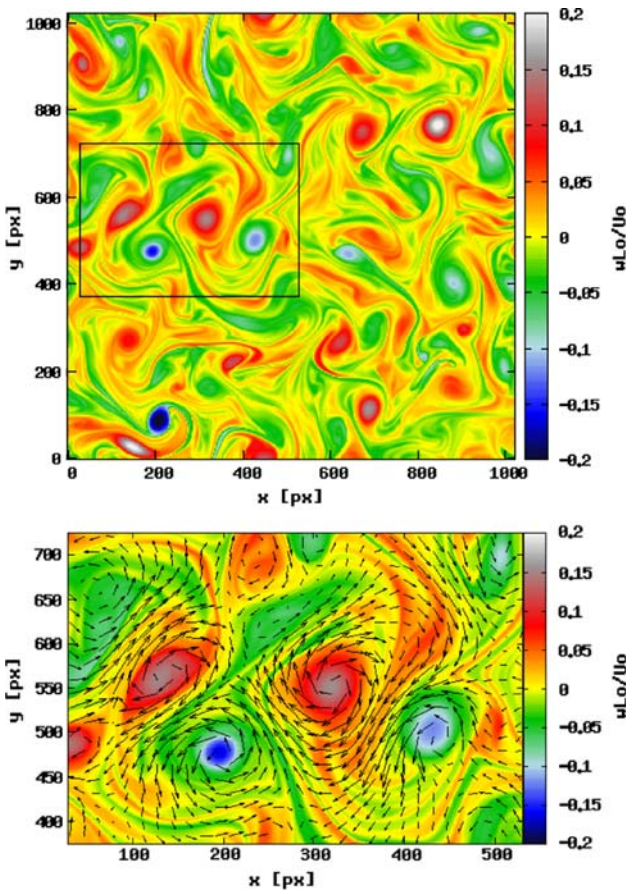

Fig. 3 Two-dimensional turbulence test case—colormap of the normalized vorticity with superposed velocity field

the vorticity equation computation using the Runge–Kutta scheme of the DNS in order to use the intermediate velocity components. However, a bicubic interpolation of the velocity field was applied since the particles were not supposed to be located at the nodes of the grid.

In the present evaluation the image pair considered led to a maximum particle image displacement up to 6 pixels. This particle image displacement was globally optimal to minimize the RMS error provided by the variational technique. This relatively small maximum displacement necessitates a multiresolution pyramid with only two levels. However, the addition of noise in the image pairs enables to put variational techniques, involving multiresolution scheme, on the wrong track.

In order to provide more realistic conditions the signal-to-noise ratio (SNR) was increased, simulating a reduction of the power of the virtual laser (Hain and Kähler 2007). The noise was quantified with peak SNR (PSNR) which is the ratio between the maximum possible power of a signal and the power of corrupting noise that affects the fidelity of its representation. Because many signals have a very wide dynamic range, PSNR is usually expressed in terms of the logarithmic decibel scale. The PSNR is most commonly used as a measure of quality of reconstruction in image compression. The PSNR is defined as

$$\mathrm{PSNR} = 10\log_{10}\left(\frac{d^2}{\mathrm{MSE}}\right)$$

where d is the dynamic of the grey level of the signal, here the particles. For an image where the particle are represented over 8 bits $d = 2^8 - 1 = 255$. MSE is the mean squared error, which for two $m \times n$ images I_o and I_r where one of the images is considered a noisy approximation of the other, is defined as

$$\mathrm{MSE} = \frac{1}{mn}\sum_{i=0}^{m-1}\sum_{j=0}^{n-1}||I_o(i,j) - I_r(i,j)||^2$$

Typical PSNR values for images of good quality lie between 30 and 40 dB. Figure 4 shows particle images influenced by the different levels of noise used for the evaluation. In comparison with these synthetic particle images, typical real particle images recorded with a high speed camera (Photron APX) exhibit relatively low PSNR values lying between 12 and 18 dB (see Fig. 5).

5.2 Real image sequence

The collaborative approach was also applied to a particle image sequence recorded in one of the wind tunnels of the Rennes regional Center of the Cemagref. The sequence shows the near wake flow of a circular cylinder at Reynolds number $Re = 3{,}900$.

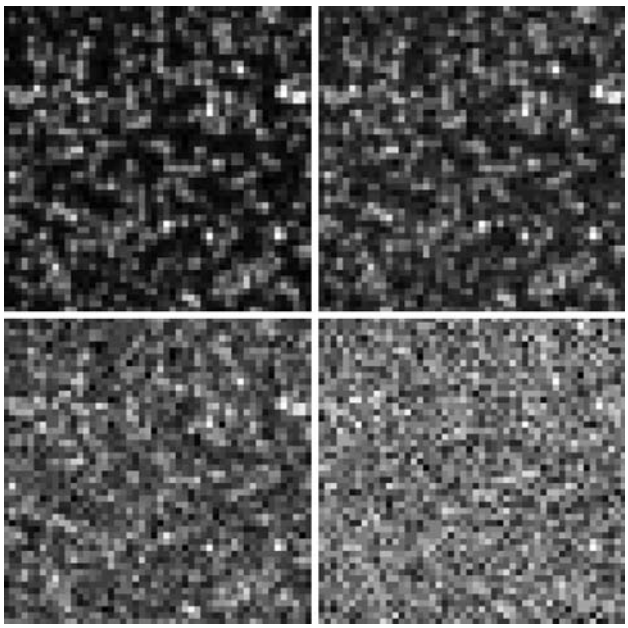

Fig. 4 Synthetic particle images (50 × 50 pixels) influenced by the reduction of the power of a virtual laser. From *left* to *right* and *top* to *bottom*, PSNR values equal 36, 24, 18 and 12 dB, respectively

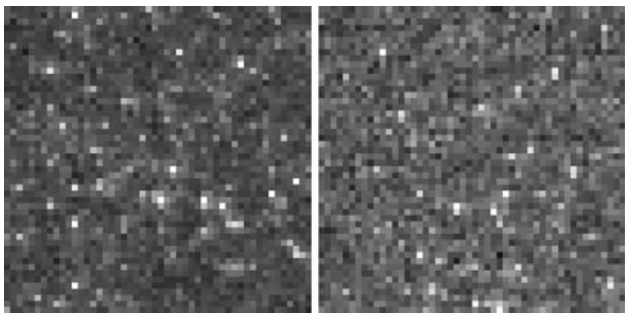

Fig. 5 Particle image pair (50 × 50 pixels) recorded with a high speed camera (Photron APX)

The circular cylinder had a length $L = 280$ mm and a diameter $D = 12$ mm. It was equipped with two thin rectangular end plates with the specification recommended by Stansby (1974). The distance between the end-plates was 240 mm providing an aspect ratio $L/D = 20$. The blockage ratio was 4.3%. The circular cylinder was mounted horizontally at $3.5D$ from the entrance of the testing zone. The free-stream velocity was adjusted at 4.8 m s^{-1}.

2D2C PIV experiments were carried out with a LaVision commercial system including a NewWave laser Solo 3 Nd-YAG (Energy by pulse of 50 mJ) and 2 PCO cameras SensiCam (CCD size of 1,280 × 1,024 pixels, pixel size of 6.7 × 6.7 μm^2 and dynamics of 12 bits). A lens with focal length of 50 mm and aperture of 5.6 was mounted on the camera. The field of view was $3.6D \times 2.9D$. The diameter

of the particle seeding (diluted polyglycol in water) were estimated to be less than 10 μm. Given the image magnification (0.2), lens aperture and light wavelength, the images of the seeding particles are diffraction limited with a diameter of 1–2 pixels in diameter.

The correlation-based velocity fields were calculated with the commercial software DaVis 6.2 from LaVision. A multipass algorithm with a final interrogation window size of 16×16 pixels and 50% overlapping was applied. Image deformation and round Gaussian weighting function were used. Spurious velocities were identified with median filter, each vector component is checked independently and replaced by the median following Westerweel (1994).

This investigation of the near wake flow is described in detail in Parnaudeau et al. (2008).

5.3 Multiresolution limitations

In Fig. 6 the total RMS error of the approaches is given as a function of the time for five image sequences characterized by different SNR. The same velocity field was used to generate the five image sequences. For all methods the RMS error was increasing with decreasing values of PSNR (increasing noise). For images of poor quality (i.e. PSNR = 12 dB), the large error observed for the multiresolution approach was mainly explained by the inaccurate estimation of the large displacements. Figure 7 clearly illustrates this behaviour. It shows the vector field of the exact solution for region of large displacements (larger than 2 pixels) and the colormap of the deviation of optical-flow from the exact velocity modulus. For regions of large velocities the deviation from the exact solution was larger than equal to 1 pixel. The corresponding RMS error, out of the range of the Fig. 6, was equal to 1.2 pixel. Small particles with large displacements in the images were

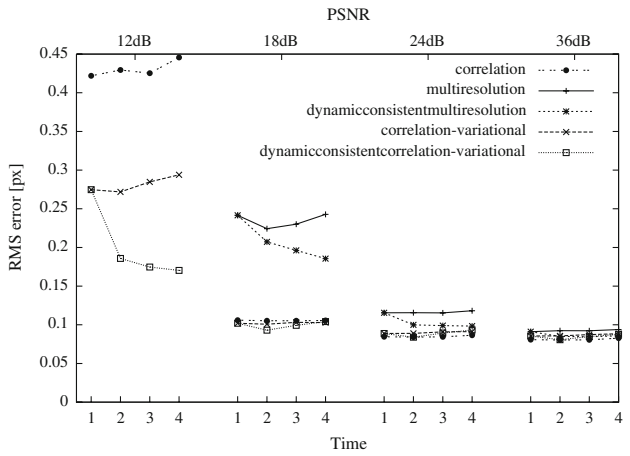

Fig. 6 Effect of the noise on the total RMS error for the different approaches and during the image sequences

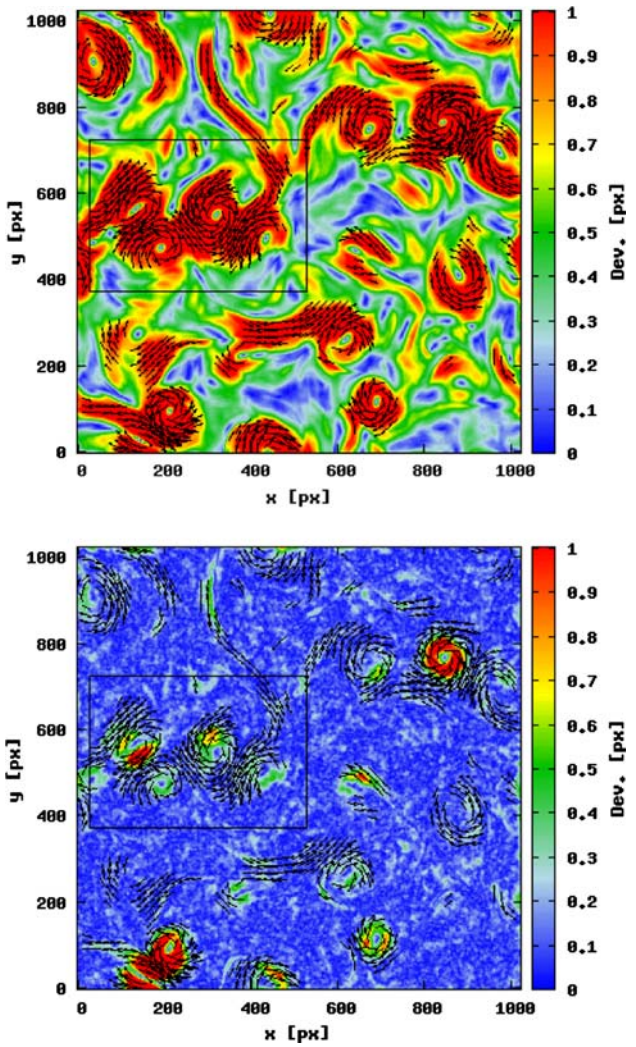

Fig. 7 Colormap of the deviation of the multiresolution approach from the exact velocity modulus—vector field of the exact solution for displacements larger than 2 pixels. *Top* PSNR = 12 dB, *bottom* PSNR = 18 dB

smoothed out by the down sampling of the multiresolution scheme. In these regions the real motion information was lost. As illustrated in Fig. 7, through the results of PSNR equal to 18 and 12 dB, this effect was further promoted by the addition of noise in the images.

The inaccurate estimation of the large displacements led to a poor extraction of the dynamics especially at large scales. Energy spectra reported in Fig. 8 give a quick view of the distribution of energy at different scales for different level of noise in the images. For PSNR = 12 dB, the multiresolution approach completely failed to estimate the dynamics in the flow. For PSNR = 18 dB and for larger values of the SNR, the multiresolution showed consistent energy distributions across the scales. Spectra of the error (difference between the multiresolution's estimation and the DNS solution) are also shown in Fig. 8 indicating an

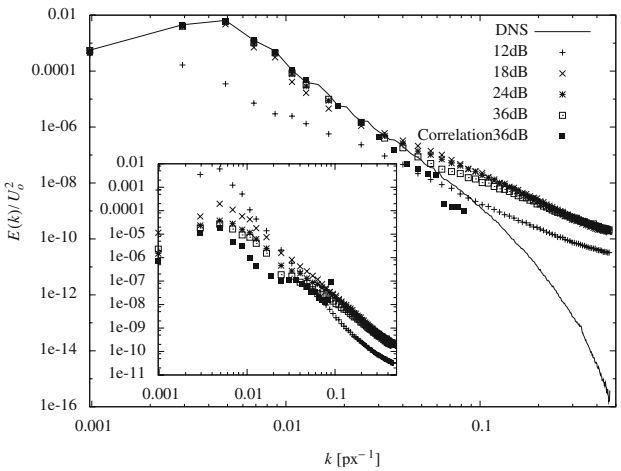

Fig. 8 Spectral response of the multiresolution approach for different levels of noise in the images. Spectra of the error for the same data are shown in *inset*

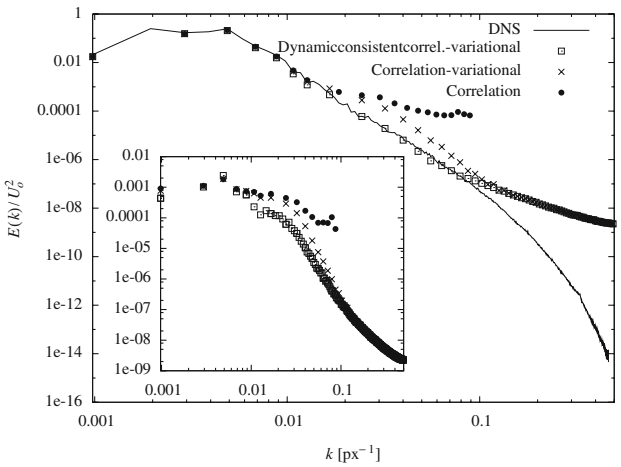

Fig. 9 Spectral response of different approaches for PSNR = 12 dB. Spectra of the error for the same data are shown in *inset*

improvement of the estimations with decreasing noise in the images. Inspection shows that the variational approach does not yields any windowing effect as it is observed for the correlation in the form of a sinc function, visible at small scales (for $k = 1/16 = 0.0625$). The monotonically vanishing error spectra provided by the variational approach clearly exhibit that the dense information estimated was consistent with the DNS reference down to the smallest scales. These behaviours can also be seen with the results of the third international PIV Challenge for the variational approach of Corpetti et al. (2006) and the correlation techniques (see Figs. 1–17 in Stanislas et al. 2008) (Fig. 9).

The accuracy of the small scales dynamics is directly linked with the regularization involved to tackle the aperture problem. The regularization is conducted from the beginning of the minimization process and complement the information of the data term with a spatial coherence. Hence, this global variational technique extracts dense vector fields (one vector per pixel), beyond the density associated to the particles. We will see in the following that the introduction of physics-based regularization can improve the estimation of the vortex dynamics at small scales. Further informations about this subject can be found in Heitz et al. (2008).

5.4 Correlation-variational approach

As shown in Fig. 6 the combined correlation-variational approach resulted in lower RMS error. Compared to the correlation method, the proposed technique allowed the estimation of the large displacements with a lower deviation from the exact velocity modulus (see Fig. 10). The improvement that could be gained with the proposed approach is exhibited in Fig. 9, giving the distribution of the energy estimated across the spatial scales. The error spectra plotted in inset shows that the combined scheme smoothed out the window effect due to the correlation. The benefit of the combined technique was especially observed for image sequences with large noise. However, for images with less noise, the colormap of the deviation from the exact velocity modulus plotted in Fig. 11, indicates that the proposed approach yielded a finer description of the vortex filaments. In the present study, as given by the parameters we manually set for best performance, the contribution of the data term of the variational approach was poor and the proposed correlation-variational global scheme behaved mainly as a regularizer of the correlation vector fields, denoising the vector fields and giving an enlargement of the dynamics. As already discussed above, the second-order variational technique used in this study gives results comparable with the most performing correlation techniques. Better performances, i.e. enlarged dynamic range with high accuracy, could be provided by the global variational scheme proposed by Yuan et al. (2007), using mimetic finite difference to compute second-order regularization, or other physics-based regularization techniques (Heitz et al. 2008).

The combined variational-correlation scheme was also evaluated with real images of turbulent flows. Figure 12 shows the estimated velocity fields using variational technique with multiresolution and the proposed correlation-variational approach. The multiresolution method under-estimated the external high velocity which was approximately two times smaller than the ground truth. This large error was reduced significantly by using the proposed collaborative approach. It should be noticed that in Corpetti et al. (2006) the same multiresolution technique succeeded in estimating the fluid motions in comparable

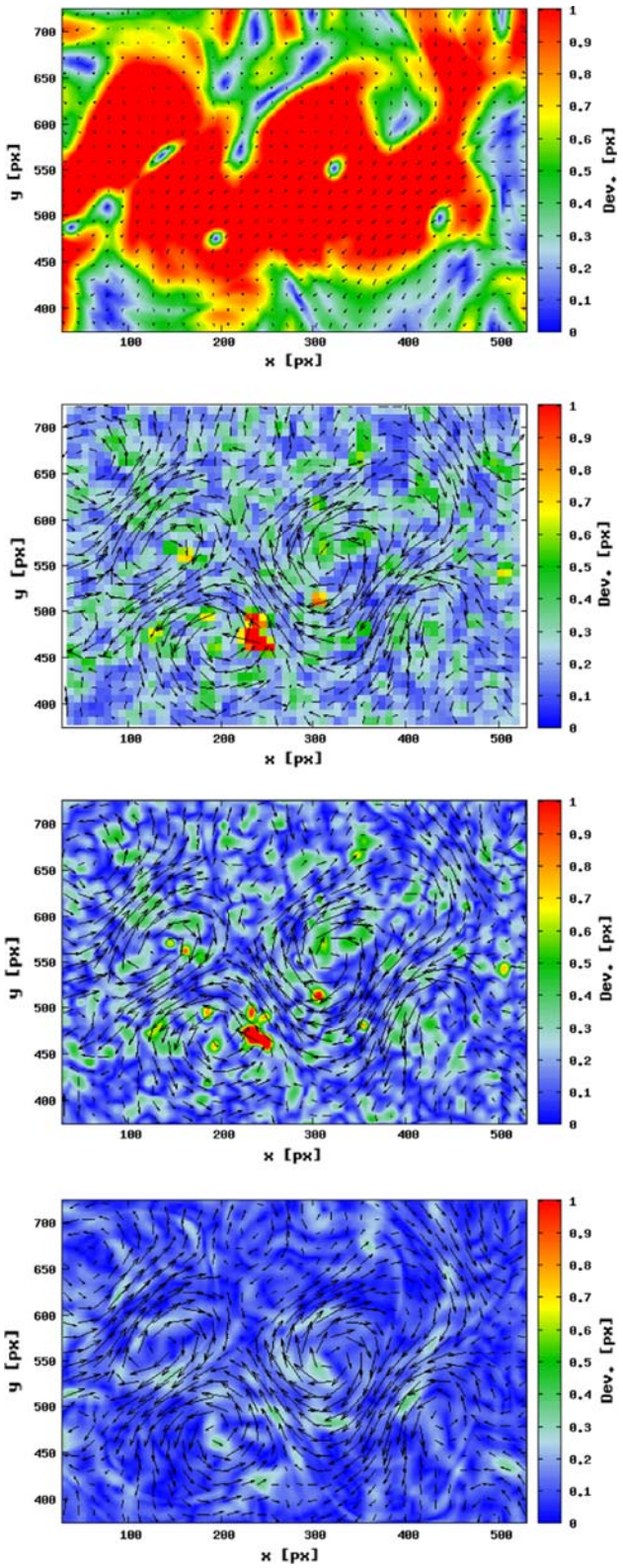

Fig. 10 Deviation of different approaches from the exact velocity modulus and corresponding vector field—from *top* to *bottom* militarisation, correlation, correlation-variational, dynamic consistent correlation-variational. PSNR = 12 dB

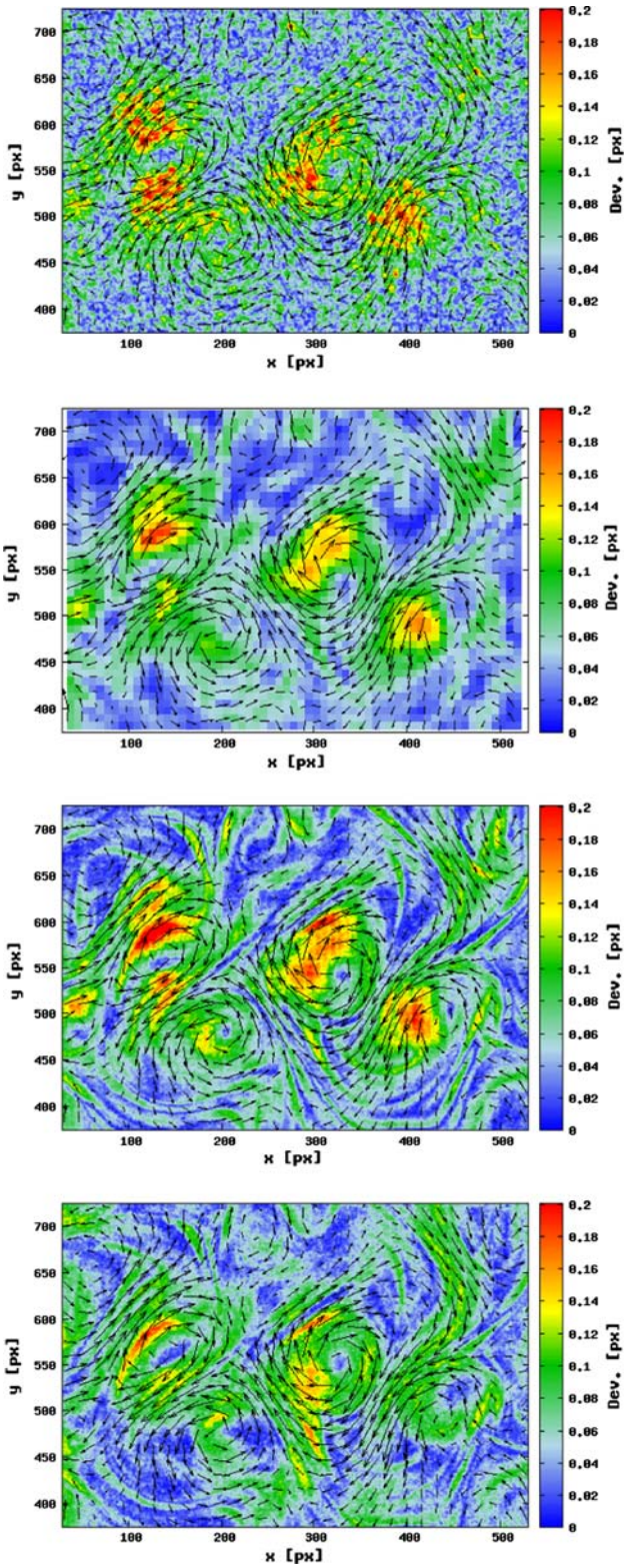

Fig. 11 Deviation of different approaches from the exact velocity modulus and corresponding vector field—From *top* to *bottom* multiresolution, correlation, correlation-variational, dynamic consistent correlation-variational. PSNR = 36 dB

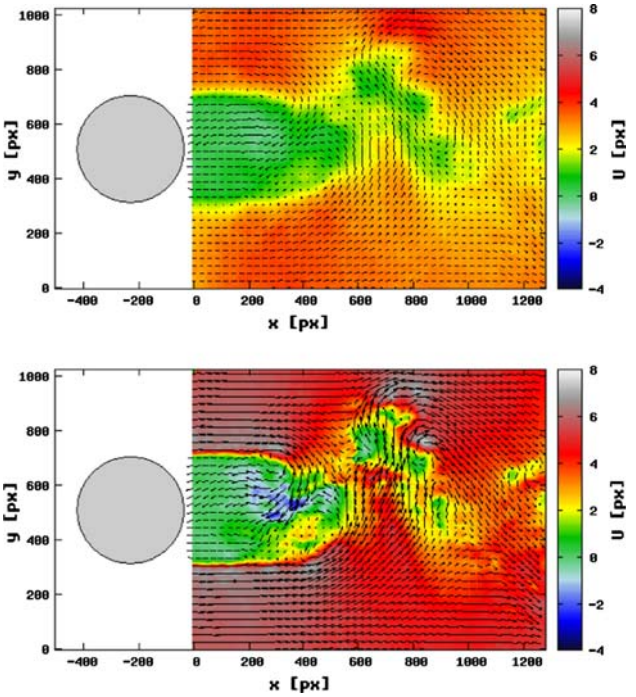

Fig. 12 Instantaneous vector field with horizontal velocity color map, in near the wake of a circular cylinder at $Re = 3{,}900$. *Top* optical-flow approach (Corpetti et al. 2006), *bottom* proposed collaborative approach

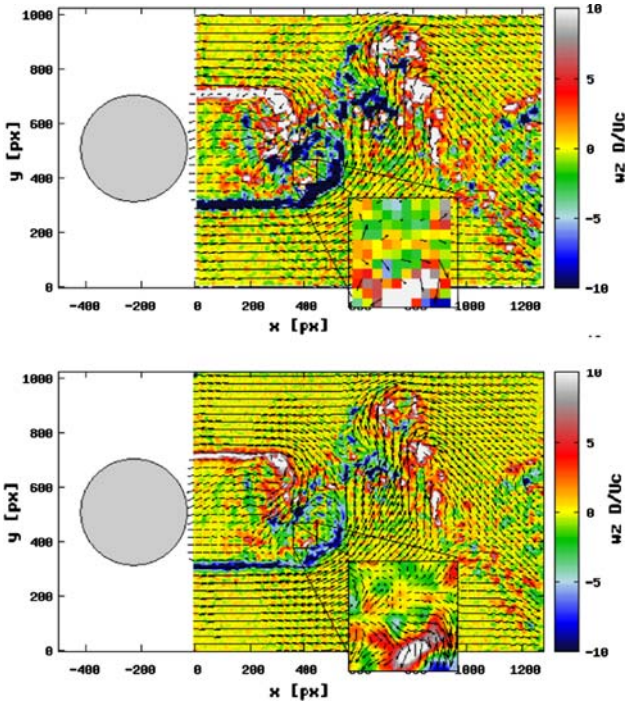

Fig. 13 Instantaneous vector field with vorticity colormap, in the near wake of a circular cylinder at $Re = 3{,}900$. *Top* correlation approach, *bottom* proposed collaborative approach

wake flow. However, in that experiment the observed particle diameters were around 3–4 pixels, whereas in the present case they were around 1–2 pixels. In Fig. 13, the vorticity colormaps of correlation-based and combined approaches are shown. Although the vorticity was computed on the finest grid provided by each methods (8 pixels for the correlation and 1 pixel for the collaborative technique), less noisy vorticity maps are obtained by the combined scheme, associated with a finer description of the flow. This evaluation with experimental data indicates that the proposed collaborative approach yielded reliable results where classical optical flow techniques failed, with an enlargement towards small spatial scales compared to correlation-based technique.

5.5 Spatio-temporal regularization

As shown in Fig. 9 for images with large noise, the improvement of the estimation with the addition of the dynamic consistency is quite efficient. The enlargement of the dynamic range resolved was almost of one decade. In addition, the computational cost associated to this spatio-temporal regularization was rather low (four times less) compared to the computation cost of the correlation-variational step. However, this computational cost could be larger if the time separation between the images was

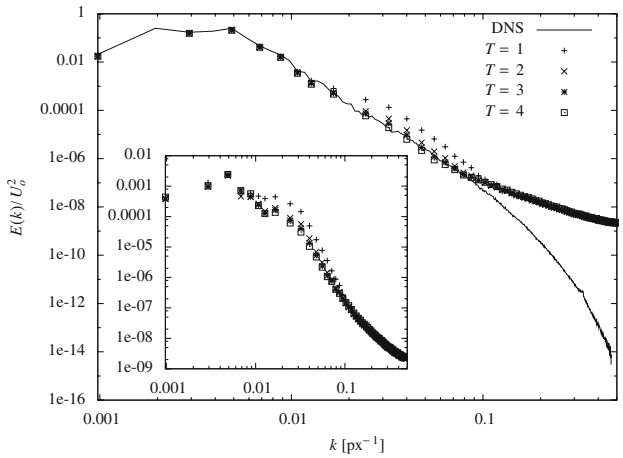

Fig. 14 Spectral response of the dynamic consistent correlation-variational approach during the image sequence for PSNR = 12 dB. Spectra of the error for the same data are shown in *inset*

increased, like in some real-time PIV experiments. The decay of the RMS observed in Fig. 6, indicated that the proposed approach was able to enhance the estimations over several frames, the main improvement being provided from the first to the second frame. During the following time steps the spatio-temporal regularization enhanced the descriptions of the spatial scales ranging between 30 and 10 pixels, corresponding to the size of

the vortices shown in Fig. 3. This phenomenon was also observed in the distribution of spectra during the time sequence, plotted in Fig. 14 and in the low deviation from the exact velocity given in the Fig. 10 where less spurious vectors can be seen compared to the other approaches.

6 Conclusion

In this paper, we have proposed and evaluated a new method for robust and dense estimations of instantaneous velocities of fluid flows from image sequences. This method is a collaborative approach satisfying Navier–Stokes equations and combining variational methods with correlation technique. The novel scheme has been specifically designed to provide physics-based, robust over noise and dense estimations. For laser sheet illuminated particle images of 3D turbulent flows a dynamic model has been derived from Navier–Stokes equations following shallow flow assumptions.

The developed approach has been tested on synthetic particle images based on 2D turbulence and on real image sequence recorded in the wake of a circular cylinder. In each cases, we compared our results with the ones issued from PIV and optic-flow. It was pointed out that for image sequence with large noise the collaborative scheme re-enforced fluid dedicated variational methods towards robustness, enlarging the range of scales that can be resolved with correlation-based techniques.

Acknowledgments The financial support by the Region of Bretagne in France under Grant No. 20048347 and by the European Union under Grant No. FP6-513663 are gratefully acknowledged.

References

Alvarez L, Castano C, García M, Krissian K, Mazorra L, Salgado A, Sánchez J (2008) Variational second order flow estimation for PIV sequences. Exp Fluids 44(2):291–304

Bergen J, Anadan P, Anna K, Hingorani R (1992) Hierarchical model-based motion estimation. In: Sandini G (ed) Proceedings of European conference on computer vision. Springer, Heidelberg, pp 237–252

Bigün J, Granlund G (1988) Optical flow based on the inertia matrix in the frequency domain. In: Proceedings of SSAB symposium on picture processing. Lund, Sweden

Black M, Anandan P (1996) The robust estimation of multiple motions: parametric and piecewise-smooth flow fields 63(1):75–104

Bruhn A, Weickert J, Schnörr C (2005) Lucas/Kanade meets Horn/Schunck: combining local and global optic flow methods. Int J Comput Vis 63(3):211–231

Carlier J, Wieneke B (2005) Report 1 on production and diffusion of fluid mechanics images and data, Fluid project deliverable 1.2. European Project 'Fluid image analisys and description' (FLUID). http://www.fluid.irisa.fr/

Corpetti T, Mémin E, Pérez P (2002) Dense estimation of fluid flows. IEEE Trans Pattern Anal Mach Intell 24(3):365–380

Corpetti T, Heitz D, Arroyo G, Mémin E, Santa-Cruz A (2006) Fluid experimental flow estimation based on an optical-flow scheme. Exp Fluids 40:80–97

Cuzol A, Hellier P, Mémin E (2007) A low dimensional fluid motion estimator. Int J Comput Vis 75(3):329–349

Hain R, Kähler C (2007) Fundamentals of multiframe particle image velocimetry (PIV). Exp Fluids 42:575–587

Héas P, Mémin E, Papadakis N, Szantai A (2007) Layered estimation of atmospheric mesoscale dynamics from satellite imagery. IEEE Trans Geosci Remote Sens (in press)

Heitz D, Mémin E, Schnörr C (2008) Fluid flow motion measurements from image sequence: a review and some perspectives. Exp Fluids (submitted)

Horn B, Schunck B (1981) Determining optical flow. Artif Intell 17:185–203

Kohlberger T, Mémin E, Schnörr C (2003) Variational dense motion estimation using the Helmholtz decomposition. In: Griffin L, Lillholm M (eds) Scale space methods in computer vision LNCS, vol 2695. Springer, Berlin, pp 432–448

Lecordier B, Westerweel J (2003) The EUROPIV synthetic image generator (SIG). In: Stanislas M, Westerweel J, Kompenhans J (eds) Particle image velocimetry: recent improvements. EUROPIV 2 workshop, Springer, pp 145–162

Liu T, Shen L (2008) Fluid flow and optical flow. J Fluid Mech (in press)

Lucas B, Kanade T (1981) An iterative image registration technique with application to stereo vision. In: Proceedings of seventh international joint conference on artificial intelligence, Vancouver, Canada, pp 674–679

Mansour NN, Ferziger JH, Reynolds WC (1978) Large-eddy simulation of a turbulent mixing layer. Technical report. Report TF-11, Thermosciences Division, Department of Mechanical Engineering, Standford University

Okuno T, Sugii Y, Nishio S (2000) Image measurement of flow field using physics-based dynamic model. Meas Sci Technol 11:667–676

Papadakis N, Corpetti T, Mémin E (2007) Dynamically consistent optical flow estimation. In: IEEE international conference on computer vision, ICCV'07. Rio de Janeiro, Brazil

Parnaudeau P, Carlier J, Heitz D, Lamballais E (2008) Experimental and numerical studies of the flow over a circular cylinder at Reynolds number 3900. Phys Fluids 20(085101). doi: 10.1063/1.2957018

Rhunau P, Schnörr C (2007) Optical Stokes flow estimation: an imaging based control approach. Exp Fluids 42:61–78

Rhunau P, Stahl A, Schnörr C (2007) Variational estimation of experimental fluid flows with physycs-based spatio-temporal regularization. Meas Sci Technol 18:755–763

Ruhnau P, Kohlberger T, Schnörr C, Nobach H (2005) Variational optical flow estimation for particle image velocimetry. Exp Fluids 38:21–32

Saint-Venant A (1871) Theorie du mouvement non-permanent des eaux, avec application aux crues des rivieres et l'introduction des marees dans leur lit. C R Acad Sci Paris 73:147–154

Stanislas M, Okamoto K, Kähler CJ, Westerweel J, Scarano F (2008) Main results of the third international PIV challenge. Exp Fluids 45(1):27–71

Stansby PK (1974) The effect of end plates on the pressure coefficient of a circular cylinder. R Aeronaut J 78:36–37

Suter D (1994) Motion estimation and vector splines. Seattle, USA, pp 939–942

Tikhonov AN, Arsenin VY (1977) Solutions of ill-posed problems. In: Scripta series in mathematics, chap II. ISBN 0470991240

Weickert J, Schnörr C (2001) Variational optic flow computation with a spatio-temporal smoothness constraint. J Math Imaging Vis 14(3):245–255

Westerweel J (1994) Efficient detection of spurious vectors in particle image velocimetry data sets. Exp Fluids 16:236–247

Yuan J, Schnörr C, Mémin E (2007) Discrete orthogonal decomposition and variational fluid flow estimation. J Math Imaging Vis 28:67–80